Aeroelastic Effects of a Very Flexible Transonic Wing: Fluid-Structure Interaction Study

Dario Aresta
dario.aresta@tecnico.ulisboa.pt
Instituto Superior Técnico, Universidade de Lisboa, Portugal

November 2017

Abstract

The challenging requirements of the transportation sector target a more efficient fuel consumption, leading to slender wing design. Because of the longer extension, the new configurations exhibit much higher deformations. Therefore, it is necessary to predict the influences in the flight performances, especially in transonic speeds, where instability problems such as flutter occur. This work performs a computational aeroelastic study of a three-dimensional transonic wing model, part of the FP7-NOVEMOR project. In order to reach this goal, a new partitioned Fluid-Structure Interaction (FSI) solver have been compiled, starting from Open-source software. It has been tested with an incompressible flow benchmark and then extended to high speed flows. The final results show large displacements, leading to a clear motion of the shocks waves along the wing chord and great variation in the flight performances.
Keywords: Fluid-Structure Interaction, Partitioned, Transonic, Aeroelasticity

Introduction

The transport sector is nowadays challenging the new requests of the international community. The innovation, demanded by the European Commission with the Horizon 2020 proposal, seek a more sustainable and resource efficient transport. In order to reduce the induced drag, hence to improve fuel consumption, a clear trend in aircraft design is the increased aspect-ratio of the wing. The new configurations usually expose a slender and lightweight structure to airflow loads that induce an high deformation and fluctuations. In this case a flight performance analysis requires more sophisticated methods than a linear analysis adopted in small deformation case, yielding to a nonlinear aeroelastic study [2]. A common way to perform aeroelastic studies is to couple a computational structural dynamics solver with an unsteady aerodynamic code using linearized schemes. This thesis focuses on the interesting and debated aeroelastic behavior of a general aviation wing in transonic flow. In the transonic flight regime, a nonlinear response approach should be preferred because of the motion of the shock waves that play an important role in the stability prediction [18]. For the scope of this work, a more comprehensive method have been adopted, in order to develop a code that is versatile to different flow Mach numbers.

FSI interactions have been studied since they gained the interest of the engineering community. The early stages of coupled systems analysis started with the firsts studies of deforming spatial domain. Later, researches regarding numerical methods applied to fluid-structure interaction (FSI) [10, 15] investigated different approaches that range from segregated to monolithic schemes starting the general framework that, even nowadays, is under study and development.

Regarding the aerospace sector, fluid-structure interaction studies have been developed to provide a good investigation method that address the aeroelastic phenomena, such as flutter and divergence [3]. In this sense, different studies in transonic windtunnel observed the limit cycle oscillations regime and compared the experimental data with computational analyses. The conclusion was that it is required a detailed structural wing model to predict a correct motion [19].

In order to perform FSI analysis for a transonic wing, a preliminary partitioned algorithm is presented and tested in the Turek's benchmark problem [21]. Then, the wing case is introduced with a geometrical description and the flight condition is defined along with computational analyses for the fluid and the structure model defined. Finally, aeroelastic studies are performed.

Aeroelastic Framework

The development of a new FSI software can be greatly fasten thanks to the use of preexistent soft-

wares with similar applications. The author preferred Open-source softwares because of the openness of their codes to new implementation and the presence of an active community of developers that share their experience. *OpenFOAM* (for "Open source Field Operation And Manipulation") was selected as fluid solver, thanks to its wide range of fluid model supported, namely compressible/incompressible, laminar, turbulent, etc. It also includes mesh motion solvers for various applications, that is the basic of every FSI application. For the simplicity of the input files, *CalculiXv2.12* was used in this work as structural solver. This package, written by Guido Dhondt [7], can execute static and dynamic simulations. Besides this, it includes a wide range of elements and constitutive relations.

Arbitrary Lagrangian-Eulerian formulation and Dynamic Mesh Motion

Dealing with problems that simulate a dynamic and strong deformation of the continuum requires a slightly different kinematic description of the phenomena, to take into account the relation between the moving mesh and the deformed domain. In a Lagrangian description, each node of the mesh follows the material particle it belongs to, during time. This is the algorithm that is usually adopted in structural mechanics. On the contrary, an Eulerian description, popular in fluid dynamics, assumes that the nodes does not follow the particles of the flow, and remains fixed in space, during time. When it comes to FSI problems, the deformation of the structure implies some changes of the shape in the fluid domain. By the way, if the nodes of the fluid follow the deformation of the structure they will not anymore be fixed in space and will not track the displacement of the fluid particles as well. Thus, they will move in an arbitrary way, depending on the problem needing. This is an Arbitrary Lagrangian-Eulerian (ALE) description. The equations in the ALE differential form for mass, momentum and energy in the so-called *reference system*, R_ζ are:

$$\left.\frac{\partial \rho}{\partial t}\right|_\zeta + \mathbf{c}\cdot\nabla\rho = -\rho\nabla\cdot\mathbf{v}, \tag{1a}$$

$$\rho\left(\left.\frac{\partial \mathbf{v}}{\partial t}\right|_\zeta + (\mathbf{c}\cdot\nabla)\,\mathbf{v}\right) = \nabla\cdot\sigma + \rho\mathbf{b}, \tag{1b}$$

$$\rho\left(\left.\frac{\partial \mathbf{E}}{\partial t}\right|_\zeta + \mathbf{c}\cdot\nabla\mathbf{E}\right) = \nabla\cdot(\sigma\cdot\mathbf{v}) + \mathbf{v}\cdot\rho\mathbf{b}. \tag{1c}$$

In this set of equations: ρ is the mass density, $\mathbf{v}$ the material velocity, σ the Cauchy stress tensor, $\mathbf{b}$ the specific body force and E the specific total energy and c the convective velocity, that is the relative velocity between the material and the mesh [8].

Once the conservation new laws are defined, it is necessary to implement a mesh motion solver that update the mesh while keeping it as regular as possible in response to the deformation of the boundaries. In FSI problems, the motion of the boundary that represents the interface between the structure and the fluid is not known a priori, but is solution-dependent, thus the motion of the mesh must be recalculated for each time step. *OpenFOAM* includes a vertex based finite volume method for automatic mesh update that compute the motion starting from a Laplace equation with a diffusion coefficient that can varies through the domain [11]. The solution of the Laplace equation gives a regular mesh composed by lines of equal potential, that is a repositioning of the internal nodes in a way that are equidistant to the connected nodes. Thus the equation:

$$\nabla\cdot(\gamma\nabla\mathbf{u}), \tag{2}$$

is solved to find the new nodes positions. γ is the diffusion field, while $\mathbf{u}$ is the point velocity that is used to change the point position:

$$\mathbf{x}_{t+1} = \mathbf{x}_t + \mathbf{u}\Delta t. \tag{3}$$

During the simulations, the Laplacian algorithm demonstrated good performance especially using an inverse relation on the diffusivity term. This prevent bad mesh quality during the motion and overlapping of cells.

FSI algorithm

Fluid-structure interaction analysis is usually classified as a 3-field problem that involve the fluid, the structure and the motion of the mesh. The partitioned approach to FSI employs a segregated solution procedure where the fluid and structure are sequentially solved and some tools provide the communication between them. This allow to use largely developed software rather than cast the two domains in a single system, that would require a ground-up coding of the entire software. In this scheme the fluid field is solved first, then the pressure and shear forces at the interface are transfered to the solid solver and a predicted motion of the solid is computed. Then the automatic mesh solver receive as input the displacements and velocities of the structure, and give as output the new mesh. Then the process is reiterated till the end of simulation is reached.

On the interface between fluid and structure, the following relations are set:

$$\sigma^f n = \sigma^s n \qquad on\ \Gamma, \tag{4a}$$

$$\mathbf{v}^f = \mathbf{v}^s \qquad on\ \Gamma, \tag{4b}$$

to ensure the mechanical and kinematic continuity (Γ is the FSI interface), being σ the stress tensor and $\mathbf{v}$ the velocity. f stands for fluid, while s for solid.

As described here, the algorithm does not check that the predicted dynamics correspond to the actual motion of the structure. For these reason it is called loosely-coupled. Loosely coupled time advancing methods does not have a correct energy balance at the interface, so they show the so-called *added-mass* effect [5]. To ensure the correspondence between the predicted and actual motion it is necessary to apply a strongly-coupled algorithm. It consists in a corrector step through sub-iterative process that check residuals set by the user at each time step. The scheme of this procedure is illustrated in Fig.1.

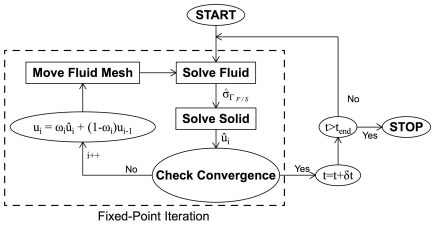

Figure 1: Strongly coupled FSI algorithm.

The relaxation step in a fixed-point iteration is given by:

$$u_i = u_{i-1} + \omega_i \left(\hat{u}_i - u_{i-1}\right) = \omega_i \hat{u}_i + \left(1 - \omega_i\right) u_{i-1}, \tag{5}$$

where i refers to the iteration number, u is the displacement applied, while $\hat{u}$ is the displacement computed by the structural solver. The relaxation factor ω_i can be constant during the sub-iterative process or can varies dynamically. Dynamic value allow for faster convergence. The Aitken scheme [14] was adopted in this work, that gives a relaxation factor equal to:

$$\begin{aligned} \omega_{i+1} &= \frac{u_{i-2} - u_{i-1}}{u_{i-2} - \hat{u}_{i-1} - u_{i-1} + \hat{u}_i} = \\ &= \omega_i \frac{u_{i-2} - \hat{u}_{i-1}}{u_{i-2} - \hat{u}_{i-1} - u_{i-1} + \hat{u}_i} = \\ &= -\omega_i \frac{r_{i-1}}{r_i - r_{i-1}} = \\ &= -\omega_i \frac{(r_{i-1})^T (r_i - r_{i-1})}{|r_i - r_{i-1}|^2}. \end{aligned} \tag{6}$$

This parameter demonstrated a good time convergence, it is easy to implement and cheap to compute. In Fig. 2 the speed of the fixed-relaxation method is compared to the Aitken's relaxation method. The results refer to the benchmark test presented later. The clear drop of number of iterations leads to a great reduction of the CPU-time in the fixed-point relaxation process.

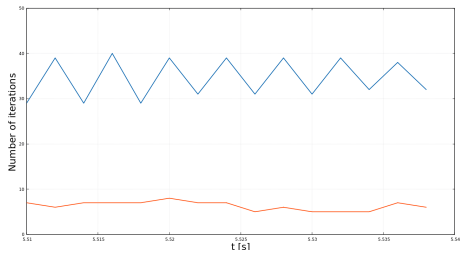

Figure 2: Comparison of the fixed-point iteration speed between fixed relaxation (blue line) and Aitken's relaxation (red line).

At the end end of each iteration, a check is executed to verify whether the inner-loop has converged or not. In this work the residuals are evaluated on the displacements:

$$u_i - u_{i-1} < \epsilon, \tag{7}$$

where ϵ is a tolerance set by the user.

The algorithm described above has been coded in an *OpenFOAM*'s new application. The code can be summarized in the following list:

1. The software starts with a pre-processing phase that finds the correspondence between the nodes and elements at the interface. This is required because, even if a conforming meshes is considered, when the elements are exported separately for fluid and structure mesh, the numbering of nodes and faces at the interface is not the same. At the beginning, the mesh corresponding to the fluid and the one corresponding to the structure are red, saving the nodes's coordinates and elements's matrix connection in different lists. Then the nodes' coordinates are compared to find a correspondence and the numbering is reordered in a way that it is the same for the different lists. Then the faces in the interface are compared to find the correspondence of the elements, to transfer the stresses.

2. Afterwards the simulation starts with the external loop, that is active till the end of the runtime. At the beginning of each time step the structure is solved. Here the interface loads are calculated as:

$$p_s = p_w, \tag{8a}$$
$$\tau_s = \rho\nu \, \nabla \mathbf{v}, \tag{8b}$$

being p_w the pressure on the generic interface face and p_s the pressure applied on the solid interface. The shear stress applied on the solid interface, τ_s, is calculated through the shear stress law for Newtonian fluids. $\nabla \mathbf{v}$ is the velocity gradient, ρ the fluid density, and ν the kinematic viscosity. Then the external structural solver is called through a system call and the predicted displacements and velocities are stored into variables.

3. After that, the sub-iterative process starts with a relaxation factor $\omega_1 = 1$. Afterwards the velocities are transferred to the mesh motion solver that computes the new positions of the nodes and the convective velocity field.

4. Now the flow field is solved.

5. At the end of the iteration a new prediction of the structure motion is computed and compared with the previous through a check on the residuals. If the iteration did not converge, the new displacements and velocities are recalculated using the Aitken's relaxation technique. The same scheme is repeated at each time step.

Benchmark

In order to verify the accuracy of the algorithm developed, a quantitative comparison with other solvers is required. Among all the literature's benchmarks, the Turek's proposal [21] was preferred because of its popularity in FSI studies. It studies a flow around an elastic body result in significant self-induced structural oscillations. The original study was conducted with a fully implicit monolithic approach. The domain consists in a simple 2D flow around a cylinder with an elastic bar attached. Referring to Fig.3 the geometry, at the start time, is fully described by the following quantities:

- The domain bounding box is $L = 2.5$ and $H = 0.41$;
- Considering the left bottom corner as the origin, the center of the cylinder is at $C = (0.2, 0.2)$ with radius $r = 0.05$. Thus the position of C gives to the geometry an asymmetrical configuration, the channel on the top of the bar is larger than the other;
- The bar is defined by the length and height, respectively $l = 0.35$ and $h = 0.02$. The right bottom corner is at $(0.6, 0.19)$;
- A control point, called A, is located at $(0.6, 0.2)$.

The model of the fluid considered is Newtonian and incompressible. Fluid properties are defined

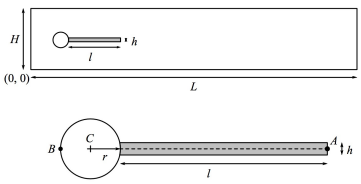

Figure 3: Geometry of the Turek's benchmark [21].

through the density ρ^f and the viscosity ν^f. A starting point for the coding of the FSI solver was *pimpleDyMFoam*, distributed with the official *OpenFOAM*'s release. This is a version of *pimpleFoam* that supports dynamic mesh. It is based on the incompressible governing equations. The equations are solved through a PIMPLE (merged PISO-SIMPLE) algorighm. It consists in a pressure-velocity coupling scheme and can be seen as a variation of the PISO (Pressure Implicit Split Operator). algorithm, with an external corrector that loops a fixed number of times defined by the user. It does support the dynamic change of the time step in order to match the desired condition on the Courant number [17].

The structure is elastic and compressible. The corresponding properties are declared as Young modulus E, Poisson ratio ν^s and the shear modulus μ^s. The equations are solved in a unconditionally stable implicit scheme in *CalculiX*.

The initial condition is a flow with velocity equal to zero. The boundary condition on the inlet is a parabolic velocity profile with a smooth increase in time, starting from a null velocity. The parabolic profile has a mean velocity $\bar{U}$. The upper and lower boundaries, as well as the cylinder and bar patches, have a no-slip condition.

Three different benchmarks have been proposed by Turek. The first results in a steady state solution, while the others show a periodic behavior in time. For the purpose of this comparison, the $FSI3$ case was reproduced. The values for the fluid and structure properties and boundary condition are recalled in Tab.1.

For this test, the Reynolds number is:

$$Re = \frac{2r\bar{U}}{\nu^f} = 200.$$

Table 1: Benchmarks's constants

Structure		**Fluid**	
$\rho^s[10^3 \frac{kg}{m^3}]$	1	$\rho^f[10^3 \frac{kg}{m^3}]$	1
$E[10^6 \frac{N}{m^2}]$	5.6	$\nu^f[10^{-3} \frac{m^2}{s}]$	1
ν^s	0.4	$\bar{U}[\frac{m}{s}]$	2

Many computational studies investigated the

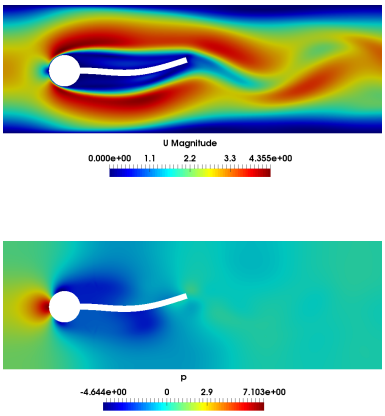

Figure 5: Mesh, velocity and pressure fields when A has maximum vertical positive displacement. Velocity and pressure in SI base unit. The pressure is referred as the incompressible value used in *OpenFOAM*, p/ρ.

transition of the wake of the flow past a circular cylinder [4]. It is well known that, even if the boundary conditions are static, the flow is not and shows periodic oscillations. To capture this flow motion, it was necessary to increase the mesh resolution. The domain have been discretized with a fully structure mesh for both structure and fluid. Respectively they have 35600 and 400 hexahedrons.

The results obtained with the FSI algorithm test are shown in Fig.4. The amplitude registered is $0.0681m$ and the frequency of $5.55Hz$. A comparison with the reference values is in Tab.2.

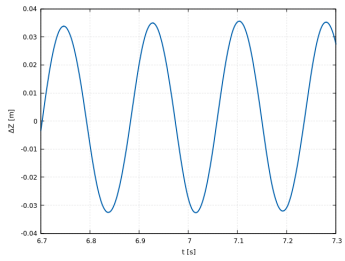

Figure 4: Vertical displacement of A in FSI test.

Table 2: Comparison with the benchmark's results.

	Calculated	**Turek**	**Error**
$\Delta z[m]$	0.0681	0.0684	0.44%
$Freq.[Hz]$	5.55	5.47	1.4%

A graphical representation of the pressure and velocity fields, when A has its maximum vertical positive displacement is displayed in Fig.5.

Wing model

The wing considered in this work is part of the FP7-NOVEMOR project (Novel Air Vehicle Configurations: From Fluttering Wings to Morphing Flight) [16]. The Reference Aircraft is a regional jet with 113 PAX in a single economic class and provide operational flexibility to fly different missions at the transonic regime. The wing geometry was defined using three different sections, distributed span-wise. The first is at the root, then one is located at the trailing-edge discontinuity and finally one at the tip. The positions of the sections, as well as the respective chords, are presented in Tab.3.

Table 3: Geometrical data of the wing.

Station	Chord $[m]$	$Y[m]$
Root	7.57	0
Break	3.99	6.18
Tip	1.73	15.73

Here, Y is the span direction. A graphical representation is provided in Fig.6.

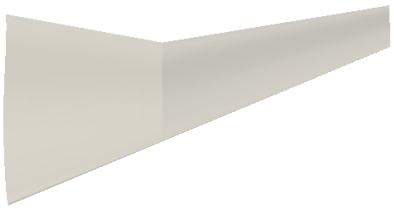

Figure 6: Top view of the transonic wing.

The geometrical model, drawn in a CAD software, has a reference area $S_w = 63.8m^2$. This will be later used to calculate the force coefficients. In external flow analysis is required to specify the geometrical boundaries that limit the domain extension. In this case a bounding box have been chosen. Supposing that the root of the airfoil is attached to one face of the box, and its center is in the origin, the bounding box extends from $(-40,\ 0,\ -40)\ m$ to $(100,\ 30,\ 40)\ m$, where the first direction is the flow direction and the second the span-wise direction. These length have been designed in a way that the boundaries's gradient are so small that there is no interaction with the flow around the wing.

Fluid model

The flight condition is transonic flight with the Mach number $M = 0.78$ and an altitude $h = 38000ft$. The standard atmosphere have been considered to evaluate the density, temperature and static pressure at this altitude [1]. The values are recalled in Tab.4.

Table 4: Flight conditions.

Altitude $[ft]$	38000
Mach	0.78
Pressure $[Pa]$	20646
Temperature $[K]$	217
Speed of sound $[m/s]$	295
Density $[kg/m^3]$	0.332

OpenFOAM's suite includes different solvers designed for high speed flows that support mesh motion. The comparison between the pressure-based *sonicFoam* and the density-based *rhoCentralFoam*, in a set of different cases that includes a flow over a wedge, a diamond airfoil and a two dimensional blunt body reveled that *rhoCentralFoam* has better performance [9]. In fact, to reproduce results of the same quality, *sonicFoam* requires three times more cells than its competitor. In compressible flows the properties are transported not only by the flow, but also by the propagation of waves. Thus the computation of the fluxes need to consider the transport in each direction. In *rhoCentralFoam* the Kurganov's method is applied [13].

Coming to the mesh definition, two chances are offered to the user: a unstructured or structured mesh. The first can be defined also as a "free" mesh, because it consists of an irregular pattern that cover the whole domain, through elements of different topology. On the other hand, a structured mesh is characterized by a "mapping" of the domain with a repeatable pattern. Even if the unstructured method allows an easy meshing of complex geometries with less interaction of the user, it usually leads to inaccuracy and non-convergence of the solution [12]. The author noticed that, in *OpenFOAM*, the higher skewness of the unstructured meshes can cause severe oscillation and crashes of the code, especially when a grading of the cells size is required to capture wall interaction. Thus, a structured mesh was preferred in this study.

In order to reduce the resources and computational time of the simulations, different meshes have been compared, to find a good trade-off between accuracy and computational cost. The number of cells and the CPU-time is presented in Tab.5. The computational time is referred to a simulation with the same boundary conditions and integration time, with an angle of attack equal to zero.

Table 5: Mesh comparison.

Mesh	Cells	CPU Time $[h]$
Fine	260694	115
Coarse	108894	27

The lift and drag coefficient, coming from the different simulations have been compared to reference values [20], in Tab.6. During the simulations a Shear Stress Transport (SST in short) $k-\omega$ turbulence model have been used.

Table 6: Force coefficient comparison, experimental data from [20].

Data	C_L	C_D
Exp.	1.30	0.0123
Fine	1.32 (1.5%)	0.0095 (22.8%)
Coarse	1.34 (3.1%)	0.0141 (14.6%)

It is clear that the run time does not exactly scale with the number of cells, it also depends on the overall quality of the mesh. A comparison of the mesh quality can be done evaluating the skewness and non orthogonality of the cells. The first measures how much, the line connecting two cell centers across the merged patches is far from the center of the face, while the other refers to the non-orthogonality between this line and the face. Tab.7 shows that the "mid" mesh is the worst in terms of skewness and number of non-orthogonal cells. Even though the finer mesh, as expected, leads to better results, the CPU-time required have been considered not compatible with a FSI analysis. For this reason the coarser mesh have been adopted for the rest of the work.

Table 7: Mesh quality comparison, *OpenFOAM*'s standard *checkMesh* utility units.

Mesh	**Max Skew.**	**Non orth. cells**
Fine	1.21	1232
Coarse	1.35	227

A plot of the Mach number in the plane of the wing root is in Fig.7. It clearly displays a first shock wave, right after the leading edge, that represents the start of the supersonic region. This ends with the second shock, allowing the flow to slow down to subsonic speeds at the trailing edge. The small number of cells adopted in the coarser mesh does not allow the strong discontinuity across the shock wave, that appears to be more like a soft variation.

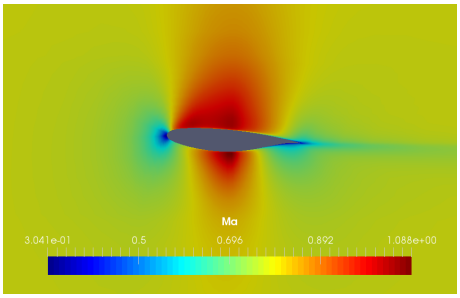

Figure 7: Mach number plot in the wing root plane

Structural model

Modern wing structures generally include spars that extend span-wise, ribs in the chord direction and stiffeners connected to the skin, plus a set of others equipments like fuel maneuvering systems, fuel tanks, engines, etc. This thesis does not aim to a comprehensive description of this complex configuration, thus a simplified discretization was preferred.

A reduced structural representation of the wing through a beam model have been investigated in other works, leading to unsatisfactory results [19]. Even though the wing geometry presented fulfill the slenderness hypothesis, the preservation of the cross-section is not. For this reason, a more complex structural model have been used.

Starting from the 2D mesh, that represents the wing skin in *OpenFOAM*, new elements have been built to increase the stiffness of the structure, and reproduce a physical bending-torsion behavior. Two-dimensional shell elements have been distributed along the chord and the span, to discretize the spars and ribs. The configuration is presented in Fig.8.

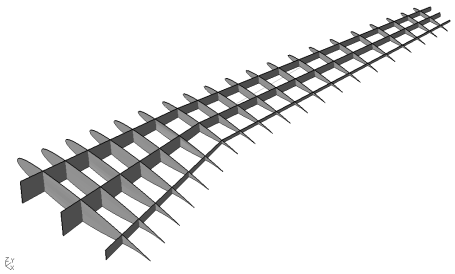

Figure 8: Wing structure model formed by 2D elements (without skin elements).

In order to predict the preferred shapes that the wing will assume during the loading, a modal analysis is performed. It finds the eigenmodes, oscillating homogeneous solutions of the linearized governing equation, and the corresponding eigenfrequencies. Fig.9 exhibits the first bending mode, and Fig.10 the first torsional mode. The second shows a strong deformation of the cross-section, that obviously does not respect the hypothesis of a beam model, where the preservation of the cross-section should be guaranteed.

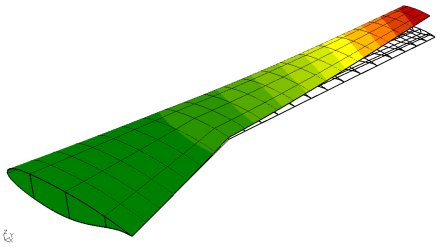

Figure 9: First bending mode, total displacements.

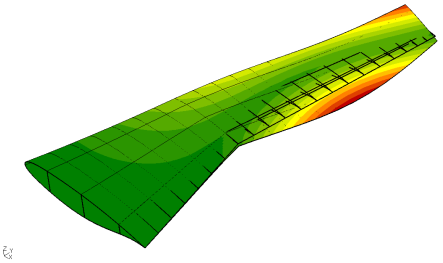

Figure 10: First torsional mode, total displacements.

Results

Even though, loosely coupled time advancing methods introduce the *added-mass* effect, the inaccuracy of this method arise in the case of internal fluid analysis of incompressible flow with comparable density value for structure and fluid [6]. Obviously, none of these hypotheses is met in the FSI transonic wing study, thus a loosely-coupled approach was preferred for the transonic wing FSI study.

Regarding the initial conditions of this analysis, the fields coming from the CFD simulations of the mesh convergence study have been transferred to this simulation. The structure was supposed to be unstressed at initial time, so the displacements are null.

In order to simulate different cases, two configuration have been considered. In particular, the thickness of the ribs and spars elements have been changed to analyze the response of wing structures with different stiffnesses. Both of them are entirely made of a material with properties similar to an aluminum alloy. The relevant mechanical properties are the elastic modulus, $E = 73GPa$, the density, $\rho^s = 2.7\ 10^3 \frac{kg}{m^3}$ and the Poisson ratio, $\nu^s = 0.33$. The two configurations are presented in Tab.8. Clearly, it is expected to have larger deformation in the second configuration, since the decreased thickness of the spars leads to a drop in the structural stiffness in both bending and torsion.

Table 8: Thicknesses of the 2D elements in the structural model.

Data	Conf. 1	Conf. 2
Skin [mm]	2	2
Rib [mm]	40	20
Spar [mm]	40	20

The displacements recorded in four points distributed along the wing surface have been stored into results to compare motion of points in the two structural configurations. Two of them are on leading edge, the other on the trailing edge. For each group one is located at the tip of the edge, the other in the middle between the tip and the wing break. For the sake of clarity, the positions are highlighted in Fig.11.

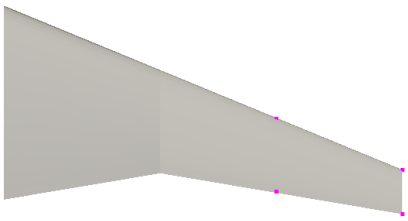

Figure 11: Positions of the four control points distributed along the wing surface.

Fig.12, Fig.13, Fig.14 and Fig.15 compare the displacements of the first configuration (in blue) with the second (in red).

As expected, the second configuration has larger displacements. In this short simulation time, a torsion deformation drives the wing motion. This is clear observing that the points on the trailing edge have positive displacements, while the ones on the leading edge have negative displacements.

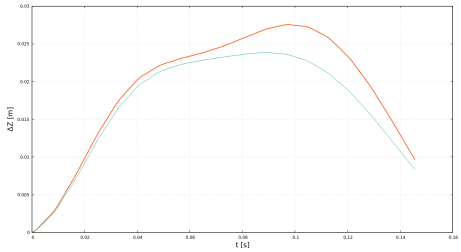

Figure 12: Displacements in the z direction for the control point on the trailing edge, at tip. Configuration 2 in red, Configuration 1 in blue.

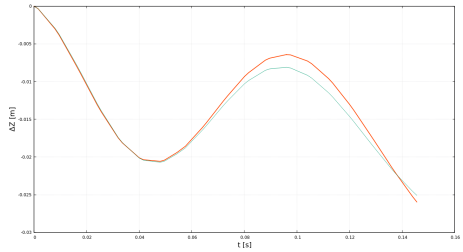

Figure 13: Displacements in the z direction for the control point on the leading edge, at tip. Configuration 2 in red, Configuration 1 in blue.

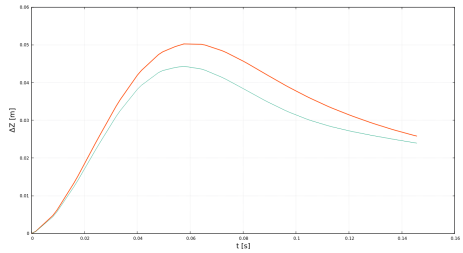

Figure 14: Displacements in the z direction for the control point on the trailing edge, between wing break and tip. Configuration 2 in red, Configuration 1 in blue.

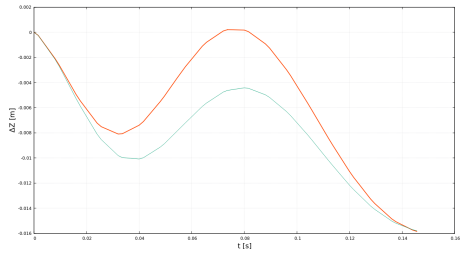

Figure 15: Displacements in the z direction for the control point on the leading edge, between wing break and tip. Configuration 2 in red, Configuration 1 in blue.

The lift and drag values during time are plotted in Fig.16 and Fig.17, respectively. The red refers to the first configuration, the ticker, while the blue lines refer to the second configuration. As expected, the larger displacements of the second configuraton lead to greater changes in both drag and lift. The torsion motion of the wing leads to a drop of 15% in the lift force during the simulation. Even though the drag force varies during time, the percentual change is much less than the one registered in the lift force. The change of the drag force, in percentage, is much lower, around 1%.

In order to describe the effects of elasticity in bending and torsion in the aerodynamics, the dynamics of the second configuration are here presented. A section at 12m from the wing root along

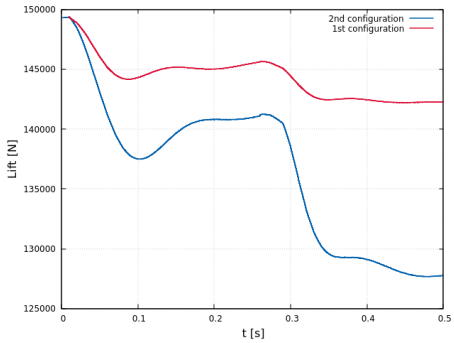

Figure 16: Plot of the lift force during the simulation.

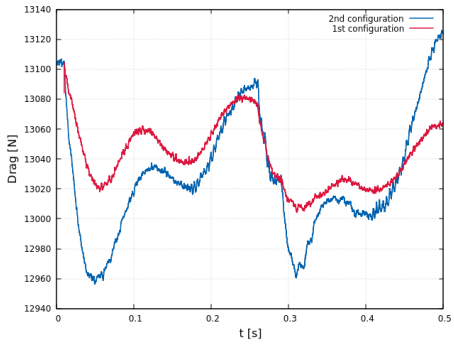

Figure 17: Plot of the drag force during the simulation.

the span direction have been selected because it is characterized by greater displacements, thus greater changes in the flow fields. The pressure field at the beginning of the simulation is presented in Fig.18 and in Fig.19 at the end of the simulation. It can be noticed that the torsional motion of this section alignes the airfoil with the upstream flow velocity, leading to a lower acceleration of the fluid along the wing surface. For this reason the shock that is in Fig.18 vanishes and become a more gentle variation of the pressure field in Fig.19.

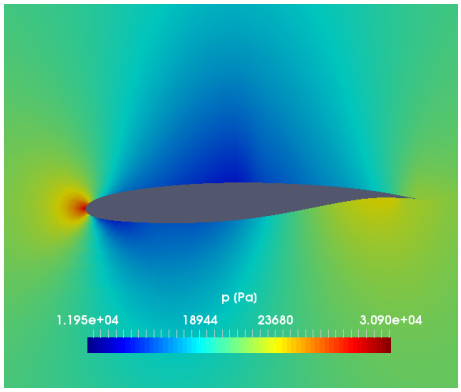

Figure 18: Plot of the pressure field at the beginning of the simulation in the selected section.

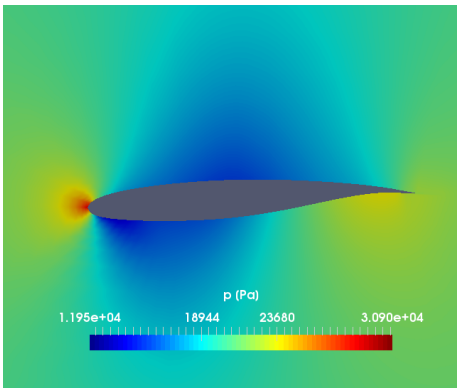

Figure 19: Plot of the pressure field at the end of the simulation in the selected section.

Conclusions

In this work different problems have been addressed, starting from the implementation of a new FSI algorithm into an open-source software environment. Even though the algorithm can be easily described through a simple flowchart, the implementation was, for some aspects, cumbersome. In this case a big help was provided by all the active developers of the open-source application employed.

Even if the analysis performed on the incompressible test has no relations with the main goal of this work, it was necessary to test if the algorithm has been implemented correctly. The good performance demonstrated on the benchmark confirmed the correctness of the whole system built.

Then, the swept wing analyzed exhibited some instabilities in the calculations because of its complex geometry. Trying different solutions, it was possible to find a meshing method, in particular the Y-block at the tip, that allowed to have stable solutions and run the transonic simulations with a relatively small number of cells.

The work is concluded with the presentation of the FSI results of the transonic wing. Even though the final results presented could be considered not satisfactory because of the short run time, the expected motion of a very flexible wing is captured. The torsional motions, especially for the second configuration leading to a drop in the lift force that is very relevant. Regarding these simulations, the very long computational time was a bottleneck for the fast advancing of the work.

The author considers that this work can be enhanced, spending more time on the following aspects:

- The support to non conformed meshes should be taken into account. In fact, the transient simulations of complex structures, like the transonic wing here discretized, can be quicken with the use of a coarser mesh at the interface;

- Thanks to the use of an external and extended structural solver, like *CalculiX*, different material models can be tested in FSI analysis, composite materials for example;
- More simulations can be executed, changing the geometry, turbulence model and flight conditions;
- The coding of an internal structural solver should be considered, calling the structural solver with a system call, as the author did in this work, does not allow to run it in parallel, thus leading to a longer computational time.
- The simulations related to the results should be continued in order to conclude this work with more details.

References

[1] International standard iso 2533. 05 1975.

[2] F. Afonso, J. Vale, E. Oliveira, F. Lau, and A. Suleman. Non-linear aeroelastic response of high aspect-ratio wings in the frequency domain. *The Aeronautical Journal*, 121:1–19, 05 2017.

[3] J. T. Batina, D. A. Bennett, Robert M.and Seidel, H. J. Cunningham, and S. R. Bland. Recent advances in transonic computational aeroelasticity. 30(1):29–37, 09 1998.

[4] S. Behara and S. Mittal. Wake transition in flow past a circular cylinder. *Physics of Fluids*, 22, 11 2010.

[5] P. Causin, J.-F. Gerbeau, and F. Nobile. Added-mass effect in the design of partitioned algorithms for fluid-structure problems. *Computer Methods in Applied Mechanics and Engineering*, 194:4506–4527, 10 2005.

[6] W. G. Dettmer and D. Perić. On the coupling between fluid flow and mesh motion in the modelling of fluid-structure interaction. *Computational Mechanics*, 43:81–90, 12 2008.

[7] G. Dhondt. Calculix crunchix users manual version 2.12. 04 2017.

[8] J. Donea, A. Huerta, J.-P. Ponthot, and A. Rodrguez-Ferran. Arbitrary lagrangian-eulerian methods. *Encyclopedia of Computational Mechanics*, 1:413–437, 11 2004.

[9] F. Gutierrez, J. Tamagno, and S. Elaskar. High speed flow simulation using openfoam. 11 2012.

[10] H. J.-P. and R. O. Morand. *Fluid-Structure Interaction: Applied Numerical Methods*. 1995.

[11] H. Jasak and Z. Tukovic. Automatic mesh motion for the unstructured finite volume method. *Transactions of FAMENA*, 30:1–20, 11 2006.

[12] A. Javidinejad. Fea practical illustration of mesh-quality-results differences between structured mesh and unstructured mesh. *ISRN Mechanical Engineering*, 2012, 07 2012.

[13] A. Kurganov and E. Tadmor. New high-resolution central schemes for nonlinear conservation laws and convectiondiffusion equations. *Journal of Computational Physics*, 160(1):241–282, 2000.

[14] U. Kttler and W. Wall. Fixed-point fluid-structure interaction solvers with dynamic relaxation. *Computational Mechanics*, 43:61–72, 01 2008.

[15] C. Michler, E. van Brummelen, S. Hulshoff, and R. de Borst. The relevance of conservation for stability and accuracy of numerical methods for fluidstructure interaction. *Computer Methods in Applied Mechanics and Engineering*, 192(37):4195–4215, 09 2003.

[16] S. Ricci, A. De Gaspari, A. Antunes, F. Odaguil, and G. Rodrigues de Lima. Application of active camber morphing concept to a regional aircraft, 01 2014.

[17] E. Robertson, V. Choudhury, S. Bhushan, and D. Walters. Validation of openfoam numerical methods and turbulence models for incompressible bluff body flows. *Computers and Fluids*, 123:122–145, 12 2015.

[18] R. G. A. Silva, J. L. F. Azevedo, and O. A. F. Mello. An investigation on viscous effects in downwash weighting methods for transonic aeroelastic stability analysis. *Journal of the Brazilian Society of Mechanical Sciences and Engineering*, 35(2):153–162, 06 2013.

[19] B. Stickan, J. Dillinger, and G. Schewe. Computational aeroelastic investigation of a transonic limit-cycle-oscillation experiment at a transport aircraft wing model. *Journal of Fluids and Structures*, 49(Supplement C):223–241, 08 2014.

[20] S. Tuling and M. Morelli. Novemor d5.2: Test report for the transonic wind-tunnel tests, 2015.

[21] S. Turek and J. Hron. Proposal for numerical benchmarking of fluidstructure interaction between an elastic object and laminar incompressible flow. *Fluid-Structure Interaction: Modelling, Simulation, Optimisation*, 53:371–385, 06 2007.